Low Temperature Physics/Fizika Nizkikh Temperatur, 2019, v. 45, No. 6, pp. 789–803

Hydrogen atom catalyzed ortho-to-para conversion in solid molecular hydrogen

A.I. Strom, K.L. Fillmore, and D. T. Anderson

Department of Chemistry, University of Wyoming, Laramie, WY 82071–3838, USA
E-mail: danderso@uwyo.edu

Received April 9, 2019, published online April 26, 2019

Infrared spectroscopy is used to investigate the process of molecular hydrogen ortho-to-para (o/p) conversion in solid hydrogen samples doped with small concentrations (10–50 ppm) of hydrogen atoms (H-atoms) as an impurity. The H-atoms are generated using the *in situ* 193 nm photolysis of N_2O dopant molecules. For hydrogen crystals with relatively low initial ortho-H_2 fractions ($X_o \leq 0.03$), the o/p conversion kinetics at temperatures of 1.8 and 4.0 K follow kinetic equations developed previously for H-atom catalyzed o/p conversion. The measured H-atom catalyzed o/p conversion kinetics indicates the H-atoms are mobile under these conditions in agreement with previous ESR measurements. It has been proposed that the H-atoms diffuse by a quantum tunneling mechanism that is described as chemical diffusion. Detailed fits of the measured o/p conversion kinetic data allow the initial H-atom concentration after photolysis to be extracted assuming literature values for the H-atom recombination rate constant ($H + H \rightarrow H_2$). The measured o/p conversion kinetics show the observed o/p conversion is much less than expected based on the previously measured H-atom recombination rate constant and thus suggest that the H-atoms do not diffuse randomly through the crystal but rather diffuse preferentially in regions of high para-hydrogen content. The estimated H-atom concentrations from this study are consistent with previous ESR measurements but in conflict with kinetic studies of H-atom reactions with various dopants such as N_2O.

Keywords: solid hydrogen, quantum solid, ortho-para conversion, quantum diffusion, nuclear spin conversion, quantum mechanical tunneling.

1. Introduction

Diffusion mass transfer in solid molecular hydrogen continues to be an active area for research due to the pronounced quantum mechanical properties of this simplest molecular solid [1–3]. The diffusion of ortho-hydrogen (oH_2) [4,5], hydrogen atoms (H-atoms) [6–14], and HD impurity molecules [15–17] in solid para-hydrogen (pH_2) have all been studied at various levels of detail. The chemical instability of the H-atom makes it both the hardest and most interesting to study. The study of H-atom reactions with various dopant molecules in solid molecular hydrogen crystals at liquid helium temperatures allow for the diffusion and reactivity of H-atoms to be studied under controlled low temperature conditions [18–27]. Our group has been studying the details of a number of H-atom reactions in solid hydrogen such as $H + N_2O \rightarrow$ *cis*-HNNO $\rightarrow$ *trans*-HNNO in highly enriched (99.97%) pH_2 crystals in the 1.8 to 4.3 K temperature range [20]. For this bimolecular reaction to occur in solid pH_2 the reactants ($H + N_2O$) must diffuse next to each other. While diffusion of N_2O in solid pH_2 under these conditions is thought to be exceedingly slow, H-atoms occupy substitutional sites [28] in the solid pH_2 crystal lattice and are known to move through the crystal by a tunneling mechanism known as chemical diffusion [6–14]. This mechanism relies on repeated $H + H_2 \rightarrow H_2 + H$ tunneling reactions instead of a physical exchange between an H-atom and a neighboring H_2 molecule [13]. H-atom chemical diffusion has been known to occur [6] for some time now and has been studied using a variety of techniques [6–14]. Yet chemical diffusion relies on quantum mechanical tunneling of the H-atom from one lattice site to another and thus this diffusion mechanism is very sensitive to the specific experimental conditions. For example, at temperatures below 4.5 K the H-atom chemical diffusion rate is independent of temperature and displays a non-monotonic dependence on the oH_2 fractional concentration (X_o) [7,12]. Even more intriguing, due to the properties of quantum solids such as solid pH_2, it has long been predicted that defects such as H-atoms move through the crystal in a coherent fashion [29,30]. If true this unique diffusion mechanism could result in qualitatively new H-atom reaction kinetics with other chemical impurities and high rates of mass transfer even at temperatures well below the Debye tem-

perature (θ_D = 120 K) [3]. The most direct way to measure H-atom diffusion in solid pH_2 is based on ESR measurements of the H-atom itself [6–14]. However, our group uses exclusively Fourier transform infrared (FTIR) spectroscopy to measure the kinetics of H-atom reactions with various reactants and ESR spectroscopy is not easily implemented using our hydrogen deposition technique [31–33]. We have tried to find a way to measure the H-atom concentration using FTIR spectroscopy to better constrain potential reaction mechanisms. We have been unsuccessful in observing previously identified H-atom induced solid pH_2 transitions [34] that would allow us to monitor the H-atom concentration directly in the IR region under our reaction conditions. We therefore decided to adopt an indirect method, similar to previous studies [11], that is based on measuring the H-atom catalyzed ortho-to-para (o/p) conversion of a solid molecular hydrogen sample to extract the time dependent concentration of H-atoms in the sample.

As we have shown previously [35] the fractional oH_2 concentration of solid hydrogen, $X_o = N_{ortho}/(N_{ortho}+N_{para})$ where N is the density of molecules in the probe volume, can be measured quantitatively using FTIR spectroscopy via the intensities of specific solid hydrogen IR absorptions that are proportional to the oH_2 or pH_2 fractional concentration. Abouaf-Marguin and co-workers used FTIR spectroscopy [36–40] to study O_2 catalyzed o/p conversion of solid normal hydrogen (nH_2) co-doped with H_2O, CH_3F, and CH_4. Similarly, Shevtsov and co-workers studied O_2 catalyzed o/p conversion in nH_2 using ESR spectroscopy and developed a kinetic equation that can be used to extract the rate constant for catalyzed conversion [41,42]. Both of these research groups show in their investigations the paramagnetic O_2 impurity catalyzes o/p conversion within the solid. The heavy O_2 impurity is thought to be immobile in solid hydrogen and thus the kinetics of O_2 catalyzed o/p conversion is diffusion controlled and limited by the rate at which oH_2 diffuses next to an O_2 molecule within the solid.

The o/p conversion kinetics in solid hydrogen catalyzed by the H-atoms should be qualitatively different from O_2 because the H-atom paramagnetic catalyst is mobile even at temperatures below 4 K. Through a variety of ESR measurements [12], Kumada and coworkers examined both H-atom diffusion and recombination separately as a function of X_o at ~4 K. These measurements show that at $X_o \geq 0.1$ the H-atom recombination rate constant is consistent with the measured H-atom diffusion coefficient, while at $X_o < 0.1$ the recombination rate is too slow. This suggests that at low X_o values the H-atom recombination reaction is no longer diffusion limited but rather constrained by some other property. Momose and co-workers were the first to study the H + NO → HNO reaction in highly enriched pH_2 solids [19]. This reaction is barrierless similar to H-atom recombination and thus it was assumed to be diffusion limited where the rate constant for the reaction k_{H-NO} is directly related to the H-atom diffusion coefficient. However, the measured rate constant was 100 times larger than the rate constant for the H-atom recombination reaction under similar conditions [19]. In that paper [19] the researchers pointed out that, "The discrepancy is so obvious that further experiments may be needed to understand the rate obtained in this study".

The purpose of this study is to investigate if H-atom catalyzed o/p conversion of solid hydrogen samples can be used to indirectly measure the H-atom concentration. Specifically, we will study the H-atom catalyzed o/p conversion of pH_2 solids with $X_o \leq 0.03$ using the 193 nm *in situ* photolysis of N_2O to generate H-atoms. We chose this precursor molecule for a variety of reasons: (1) N_2O has an appreciable cross section [43,44] at 193 nm to generate O-atoms that can react with the pH_2 host to generate H-atoms, (2) 193 nm photolysis also generates N_2 co-fragments that are closed-shell and therefore cannot catalyze o/p conversion effectively, and (3) we are interested in the H + N_2O reaction that can be initiated using N_2O as a photolysis precursor [20]. It is well known from gas phase studies that [43,45],

$$N_2O + h\nu(193\ \text{nm}) \rightarrow N_2(X\ ^1\Sigma_g^+) + O(^1D) \qquad (1)$$

and thus *in situ* photolysis of N_2O generates H-atoms via subsequent fast reactions of the ejected O-atom with the pH_2 host. We know H-atoms are produced because the *in situ* photolysis generates H_2O photoproducts and because we have measured the ensuing H + N_2O reaction kinetics [20]. We chose not to use O_2 or NO as photolysis precursors for O-atoms because these species are paramagnetic and can also catalyze o/p conversion thereby complicating the interpretation of the results [36]. The work presented here builds off our previous FTIR measurements that used 355 nm photolysis of Cl_2 precursors and the IR initiated Cl + $H_2(v = 1)$ → HCl + H reaction to follow the H-atom catalyzed o/p conversion in solid hydrogen [35]. One major difference between the present studies and the Cl_2 photolysis studies is that in this case we can quickly (~6 min) generate high concentrations of H-atoms whereas the Cl-atom studies relied on IR radiation to generate H-atoms which is a slower process (100–200 min) due to the smaller fluence of the IR source [35,46]. In addition, the 355 nm Cl_2 photolysis step in these studies produce Cl-atoms that can also effectively catalyze o/p conversion starting at $X_o \approx 0.5$ as we showed [35]. The FTIR measurements presented here compliment the previous ESR measurements of H-atom catalyzed o/p conversion [10,12] and we hope to one day use the combined techniques of ESR and FTIR to investigate H-atom quantum phenomena in solid pH_2.

This paper is organized as follows. In Sec. 2 we briefly describe the model of H-atom catalyzed o/p conversion adopted here to analyze the kinetic results. In Sec. 3 we present the experimental details used to synthesize and

characterize the H-atom doped pH_2 solids. In Sec. 4 we report the results and analysis of eight different solid pH_2 samples with varying photolysis and deposition conditions. Finally, in Sec. 5 we summarize our main results and outline the outstanding questions that remain.

2. Model of H-atom catalyzed conversion in solid hydrogen

The model of H-atom catalyzed o/p conversion adopted here is based on the model developed by Shevtsov and coworkers [10] in their analogous ESR studies of H-atom catalyzed o/p conversion of nH_2. This allows us to introduce the various equations and parameters involved in these studies so it is easier to discuss the experimental results in Sec. 4.

Any analysis of H-atom catalyzed o/p conversion of solid molecular hydrogen must account for two time-dependent processes: (1) the rate of H-atom catalyzed o/p conversion and (2) the decay of the H-atom concentration via recombination and other potential chemical decay channels. In addition, the overall o/p conversion observed is the sum of the self-conversion ($oH_2 + oH_2 \rightarrow pH_2 + oH_2$) and H-atom catalyzed conversion ($H + oH_2 \rightarrow H + pH_2$) processes. To a first approximation, both o/p reactions can be considered diffusion-limited bimolecular reactions, in the first case between two diffusing oH_2 molecules, and in the second case between an H-atom and an oH_2 molecule. Furthermore, it is assumed that the diffusion of oH_2 and H-atoms is isotropic and homogenous and, thus, both diffusing species are allowed to move throughout the entire crystal lattice. Hence, the total conversion process is described by the following differential equation [10]

$$\frac{dX_o}{dt} = -k_o n_o^2 - k_{cc} n_{\mathrm{H}} n_o , \qquad (2)$$

where n_o is the number density of oH_2 in the crystal, k_o is the self-catalyzed rate constant, k_{cc} is the H-atom catalyzed rate constant, and n_{H} is the number density of H-atoms in the sample. The first term on the right-hand side of Eq. (2) accounts for the self-conversion o/p process and the second term accounts for H-atom catalyzed o/p conversion. The H-atom recombination reaction competes with the H-atom catalyzed o/p conversion, as

$$\frac{dn_H}{dt} = -2k_r n_{\mathrm{H}}^2 , \qquad (3)$$

where k_r is the rate constant for the H-atom recombination reaction. This is a textbook example of second-order kinetics with the corresponding integrated rate law [47]. If the initial concentration of H-atoms is large enough, so that $k_r n_{\mathrm{H}}(0) >> k_o n_o(0)$, then the time dependence of X_o is simply represented as follows [10]:

$$X_o(t) = \frac{X_o(0)}{\left[1 + 2k_r n_{\mathrm{H}}(0) t\right]^{\beta}} , \qquad (4)$$

where $X_o(0)$ and $n_{\mathrm{H}}(0)$ are the initial oH_2 fractional concentration and H-atom number density, respectively, and $\beta = k_{cc}/2k_r$. Thus, one expects that $X_o(t)$ (or equivalently $n_o(t)$ should decay in a similar fashion to the concentration of a reactant that is undergoing second-order kinetics, yet augmented by the β-parameter, which reflects the ratio of the relevant rate constants. From the literature [3], k_o = $= 1.22(3)\cdot 10^{-26}$ $cm^3\cdot min^{-1}\cdot mol^{-1}$. This value is typically reported [3] as 1.90(5)% h^{-1} but by using the density of solid pH_2 ($2.600\cdot 10^{22}$ $mol\cdot cm^{-3}$) we can convert it to more conventional units. The rate constant for the H-atom recombination reaction [12] at X_o = 0.01 is significantly larger at $k_r = 1.9\cdot 10^{-20}$ $cm^3\cdot min^{-1}\cdot mol^{-1}$ which reflects 1) the larger diffusion coefficient for an H-atom compared to an oH_2 molecule and 2) the faster o/p conversion rate for an H-atom with an unpaired electron compared to an oH_2 molecule with non-zero nuclear spin. The approximately million times larger k_r rate constant means that the assumption used to simplify the kinetics ($k_r n_{\mathrm{H}}(0) >> k_o X_o(0)$) should be justified even for relatively small H-atom concentrations (e.g., 5–50 ppm). However, FTIR spectroscopy cannot measure the time dependence of $n_{\mathrm{H}}(t)$ directly and thus we can only estimate $n_{\mathrm{H}}(0)$ based on least squares fits of our o/p conversion kinetic data to Eq. (4) and by extracting the $k_r n_{\mathrm{H}}(0)$ parameter from the fit. Once the parameter is determined, we can estimate the $n_{\mathrm{H}}(0)$ concentration by dividing the fitted parameter $k_r n_{\mathrm{H}}(0)$ by the literature value of k_r. This procedure allows us to estimate the initial H-atom concentration from detailed fits of the H-atom catalyzed o/p conversion kinetics, which is useful for interpreting chemical kinetics involving H-atoms as reactants.

3. Experimental

The "rapid vapor deposition" technique developed by Fajardo and Tam is employed to produce ~2 mm thick optically transparent crystals of N_2O doped solid hydrogen [31–33]. The N_2O doped hydrogen solids are grown by co-deposition of separate H_2 host (Linde Gas, purity: 99.999%) and N_2O dopant (Sigma-Aldrich Isotec, ^{15}N 98%, ^{18}O 95%) gas streams onto a BaF_2 optical substrate cooled to ~2.5 K within a liquid He bath cryostat. The pH_2 gas is deposited at an approximate flow rate of 270 $mmol\cdot h^{-1}$. Pure pH_2 is deposited for a short period of time at both the beginning and end of the crystal growth process to ensure the N_2O dopant is homogeneously distributed throughout the sample. The oH_2 content in the crystal is controlled by passing nH_2 gas through a variable low-temperature o/p converter packed with a paramagnetic $Fe(OH)_3$ catalyst during deposition. The X_o value of the solid is dictated by the thermal equilibrium established in the o/p converter during deposition because o/p conversion within solid H_2 is very slow [3]. Therefore, the X_o value in the crystal can be predicted from the temperature of the o/p converter ($T_{o/p}$) using the rotational partition function of H_2 and assuming complete nuclear spin equilibration. In this study the o/p converter is

operated at 20, 25, and 30 K producing samples with corresponding X_o values of $1.76{\cdot}10^{-3}$, $9.63{\cdot}10^{-3}$, and $29.5{\cdot}10^{-3}$, respectively.

The H-atom doped pH_2 solids are prepared via 193 nm *in situ* UV photolysis of N_2O precursor molecules. The N_2O doped pH_2 crystals are photolyzed using the 193 nm output of an ArF excimer laser operating at 250 Hz with a pulse energy of 0.38–0.54 mJ·pulse^{-1} and cross sectional area of ~50 mm^2, controlled by an iris placed in front of the cryostat. The 193 nm photolysis beam is aligned to impinge on the sample at 45° with respect to the surface normal of the substrate. Samples were photolyzed for 1.5 to 6.0 min for as-deposited samples at 1.8 K or annealed samples at 4.0 K.

IR spectra are recorded with a FTIR spectrometer (Bruker IFS-125-HR) using a transmission optical setup where the IR beam is focused through the sample with the main optical axis parallel to the substrate surface normal. Near-IR spectra at 0.03 cm^{-1} resolution are recorded from 1800 to 8000 cm^{-1} using a CaF_2 beamsplitter, tungsten source, and liquid nitrogen-cooled InSb detector. The o/p conversion kinetics is typically measured by recording spectra with 9 or 25 averages corresponding to 1.97 and 5.48 min acquisition times, respectively. In these studies, time $t = 0$ is defined as the end of the photolysis exposure and the midpoint of each FTIR scan ($t = t_0 + 0.5t_{acquisition}$) is the reported time. Note that faster acquisition times are typically used at early times post-photolysis for increased temporal resolution and then slower acquisition times (more averages) are adopted at later reaction times to improve signal-to-noise (S/N).

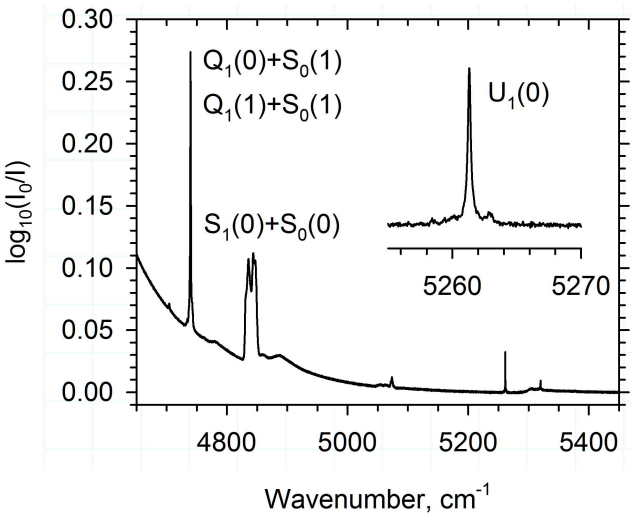

Fig. 1. Representative FTIR absorption spectrum of a N_2O doped solid pH_2 sample displaying the absorptions used in this study to monitor path length, X_o and X_{hcp}. We use the two overlapping double transitions $Q_1(0) + S_0(1)$ and $Q_1(1) + S_0(1)$ at 4736 cm^{-1} to monitor X_o, the $U_1(0)$ single transition (see inset) near 5261 cm^{-1} to monitor X_{hcp}, and the $S_1(0) + S_0(0)$ double transition at ~4840 cm^{-1} to determine the path length of the crystal. Note also visible in this region are the $S_1(1)$ transition near 4704 cm^{-1}, the $S_1(1) + S_0(0)$ transition near 5064 cm^{-1}, and the $Q_1(0) + U_0(0)$ transition near 5320 cm^{-1}. This is the spectrum of an as-deposited sample (Expt. 5) recorded at 1.82(1) K with $X_o = 0.02824(5)$, $d = 0.204(1)$ cm, and $[N_2O] = 119(1)$ ppm.

A variety of properties of the doped pH_2 solid are monitored using FTIR spectroscopy including crystal thickness, crystal structure, and X_o. Figure 1 displays a typical FTIR spectrum in the region of the absorptions used to measure various properties of the pH_2 crystal. The crystal thickness (IR path length, d) is determined using the integrated intensities of the $Q_1(0) + S_0(0)$ and/or the $S_1(0) + S_0(0)$ solid pH_2 double transitions and the proportionality constants 90(2) and 7.0(2) cm^{-2}, respectively, determined by Fajardo and co-workers [33,48]. The intensities of these double transitions are not sensitive to crystal structure and thus these absorptions are well suited for thickness measurements [33]. For all the samples studied here, the crystal thickness determined using these double transitions agreed to within 5% and, thus, reported d values are obtained from the higher S/N $Q_1(0) + S_0(0)$ double transition. We use the term "as-deposited" to refer to hydrogen samples right after deposition that have never been exposed to temperatures above ~2.5 K. The as-deposited solids are known to exhibit a mixed hexagonal-close-packed (hcp) and face-centered-cubic (fcc) crystalline morphology [49]. We can monitor the fraction of hcp crystal structures, $X_{hcp} = N_{hcp}/(N_{hcp} + N_{fcc})$, using the $U_1(0)$ single transition at 5261 cm^{-1} (see inset of Fig. 1) [50–53]. As discussed by van Kranendonk [1,54], the intensity of zero phonon single IR transitions in solid pH_2 are subject to the "cancelation effect", which arises because the dipole moments induced by intermolecular interactions between a molecule and its neighbors tend to cancel one another. Thus, the $U_1(0)$ transition is only possible for pH_2 molecules in crystal sites that lack a center of inversion (i.e., hcp) [33]. We can therefore use the following equation to measure X_{hcp},

$$X_{hcp} = 2.303 \frac{cV_0}{\tilde{\alpha} d \tilde{\nu}_0 N_A} \int_{\tilde{\nu}} \log\left[\frac{I_0(\tilde{\nu})}{I(\tilde{\nu})}\right] d\tilde{\nu}, \qquad (5)$$

where c is the speed of light, α is the absorption coefficient ($7.50(10){\cdot}10^{-17}$ cm$^3{\cdot}$s$^{-1}{\cdot}$mol^{-1}) [53], V_0 is the molar volume of solid pH_2 (23.16 cm$^3{\cdot}$mol^{-1}) [3], d is the path length, ν_0 is the peak frequency (5261.395(5) cm^{-1}) [53], N_A is the Avogadro constant, and I_0 and I are the incident and transmitted IR intensities used to calculate absorbance. Therefore, $0 \le X_{hcp} \le 1$ and should increase to near unity upon annealing because the thermodynamically more stable crystal structure is hcp.

As described previously [35], we use the overlapping $Q_1(0) + S_0(1)$ and $Q_1(1) + S_0(1)$ double transitions to monitor X_o. This double transition is shown in Fig. 1 at ~4740 cm^{-1}. This double transition is well isolated from the $S_1(1)$ peak (also shown in Fig. 1) and the integral absorption coefficient for this transition is given by

Table 1. Absorption coefficients and integration limits used in these studies

Property/species	Assignment	Intensity	ν_0, cm^{-1}	Limits, cm^{-1}	Ref.
X_o	$Q_1(0) + S_0(1)$	3900(24) cm·mol^{-1}	4739.74	4727–4750	35
X_{hcp}	$U_1(0)$	7.50(10)·10^{-17} cm^3·s^{-1}	5261.395	5258–5265	53
N_2O	$2\nu_1$	7.364 km·mol^{-1}	2446.4	2443–2451	58
N_2O	$\nu_1 + \nu_3$	10.034 km·mol^{-1}	3346.0	3342–3352	58
trans-HNNO	ν_1	47.56 km·mol^{-1}	3273.17	3270–3276	59

$$\int \tilde{\alpha} d\tilde{\nu} = aX_o^2 + bX_oX_p, \tag{6}$$

where based on the induction mechanism [55], a and b are approximately in the ratio of 1:2.5. Note the fractional pH_2 concentration, $X_p = N_{para}/(N_{ortho}+N_{para})$, is defined similarly to X_o with $0 \le X_p \le 1$. At low X_o values this peak is predominantly due to the $Q_1(0) + S_0(1)$ double transition because the contribution to the integral coefficient by the $Q_1(1) + S_0(1)$ transition decreases as the square of X_o. Thus, at low X_o values ($X_o \le 0.03$) the integrated intensity of this peak is directly proportional to X_o. Accordingly, we use the following equation:

$$X_o = 2.303\frac{V_0}{\varepsilon d}\int \log\left[\frac{I_0(\tilde{\nu})}{I(\tilde{\nu})}\right] d\tilde{\nu}, \tag{7}$$

where ε has been determined previously [35] and is reported in Table 1. At low X_o values, this analysis assumes the integrated absorption coefficient for this transition is essentially constant, thereby simplifying the analysis. Finally, the concentrations of various dopant species are determined using the following equation:

$$[X] = 2.303\frac{V_0}{\varepsilon d}\int \log\left[\frac{I_0(\tilde{\nu})}{I\tilde{\nu}}\right] d\tilde{\nu}\,(1{\cdot}10^6), \tag{8}$$

where $[X]$ is the concentration of species X in ppm and it is assumed that the gas phase integral absorption coefficient (ε values) can be used without corrections for the condensed phase environment. In this study, the $2\nu_1$ overtone and $\nu_1+\nu_3$ combination band of N_2O are used to monitor the concentration of N_2O in the range between 10 to 100 ppm. The *trans*- $H^{15}N^{15}N^{18}O$ concentration is determined using the integrated intensity of the ν_1 NH stretch vibration and the band intensities reported by Peterson at the UHF-CCSD(T)/AVQZ level of theory in a private communication for the *trans*-$H^{15}N^{15}N^{18}O$ isotopomer [20]. To be consistent with previous reports where we used the ν_2 NN stretch vibration to monitor the concentration [20], we scaled the calculated ν_2 intensity (240.2 km·mol^{-1}) by the measured ratio of integrated intensities between ν_1 and ν_2 (0.1980). The specific values of the constants used in Eqs. (5)–(8) are presented in Table 1 for both solid hydrogen properties and dopant concentrations.

4. Results and discussion

4.1. Temperature dependence of o/p conversion

In some of the early ESR [8,9] work on nH_2 it was found that k_r showed a temperature dependence that was consistent with classical H-atom diffusion behavior at temperatures above 4.75 K and quantum diffusion below 4 K. At low temperature the k_r rate constant was found to depend linearly with temperature ($k_r(T) \sim T^{0.98}$) which was interpreted as evidence of single-phonon assisted H-atom quantum diffusion [8]. More recent ESR studies [12] on enriched pH_2 samples did not measure the temperature dependence of k_r directly, but rather indirectly based on ESR linewidth and T_1 relaxation time. These studies confirm the earlier result that below 4.5 K the k_r value is temperature independent or only slowly decreasing with temperature. This is consistent with the idea that H-atom recombination is a quantum diffusion limited process, and thus, the o/p conversion kinetics is not expected to show a strong temperature dependence.

We set out to measure the H-atom catalyzed o/p conversion kinetics at 1.8 and 4.0 K. As described in the proceeding section, FTIR spectroscopy allows for a number of crystal properties to be measured simultaneously during an o/p conversion kinetic experiment. Kinetic traces of d, X_{hcp}, and X_o are shown in Fig. 2 for one of the first o/p conversion experiments conducted on an as-deposited sample at 1.775(2) K. The reported temperature is the average value and the reported error is the 1σ standard deviation. The circles are the data points extracted from individual spectra and the lines are fits to the data. This sample had an initial N_2O concentration of 47(1) ppm and was photolyzed at 212 mW·cm^{-2} for 1.5 min to initiate o/p conversion. The time and duration of the photolysis exposure is indicated by a grey line in Fig. 2. The data for d and X_{hcp} are least-squares fit to the equation of a line ($y = mt + b$), and the fitted parameters are indicated in the figure caption. Note that, as expected, both d and X_{hcp} are essentially constant over the approximately 675 min observation window. At 1.775(2) K, the pH_2 sublimation rate is negligible and thus the crystal thickness is constant within error [56]. The small increase in crystal thickness (m = 4.5(7)·10^{-6} cm·min^{-1}) over this duration likely results from changes in the integral absorption coefficient of the $Q_1(0) + S_0(0)$ double

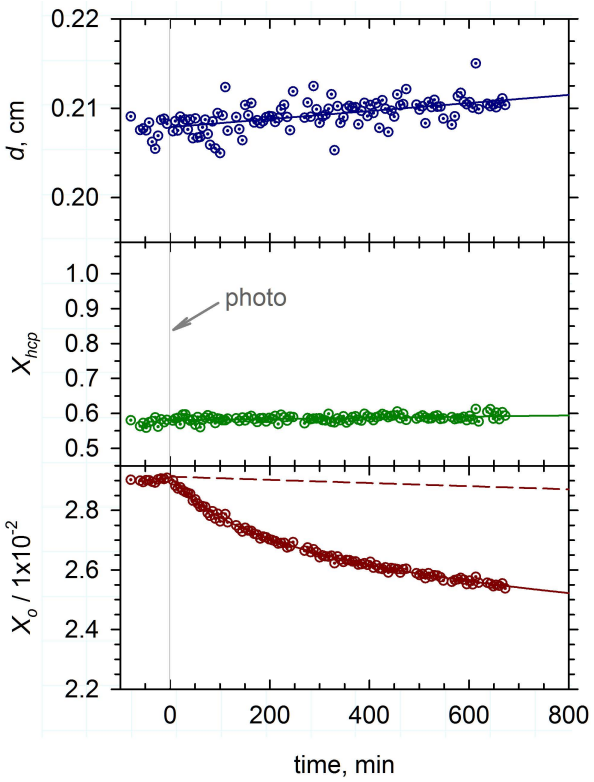

Fig. 2. (Color online) Kinetic traces illustrating the changes in d, X_{hcp}, and X_o for an experiment conducted on an as-deposited sample (Expt. 1) at 1.775(2) K. The circles are the data points and the lines are fits to the data (see text for details). The sample is photolyzed at 212 mW·cm^{-2} for 1.5 min to initiate the H-atom catalyzed o/p conversion. The dashed line shows the predicted X_o time dependence based on the self-conversion rate constant and the initial $X_o(0)$ value. The d and X_{hcp} data are fit to the equation of a line ($y = mx + b$) with $m = 4.5(7)\cdot10^{-6}$ cm·min^{-1} and $b =$ = 0.2079(2) cm for d and $m = 1.7(4)\cdot10^{-5}$ min^{-1} and $b = 0.581(2)$ for X_{hcp}.

transition used to measure thickness. The integral absorption coefficient for this particular transition is proportional to X_p^2 because [55] it involves two pH_2 molecules and thus the coefficient increases by 0.82% over the measured X_o values. Note that the thickness is not corrected for these small changes in the absorption coefficient. The X_{hcp} value of ~0.581(2) is typical of an as-deposited pH_2 sample where the crystal is almost an equal mixture of fcc and hcp crystal morphologies [33]. It was previously demonstrated that dopants can increase the fcc content by shifting the energetic balance between these two very similar crystal structures [57].

The change in X_o initiated by the 1.5 min photolysis is readily apparent. Before photolysis, the X_o value is nearly constant at 0.02907(3) which is comparable to the expected value for a pH_2 crystal grown with the $T_{o/p}$ set to 30.0 K ($X_o = 0.02947$). At these relatively low X_o values the self-conversion rate is very slow. The dashed line in Fig. 2 indicates the predicted X_o time dependence if only self-conversion is occurring [3]. Clearly the rate of o/p conversion is increased after photolysis relative to self-conversion. Another important finding is the data are well described by Eq. (4), and the fitted parameters are summarized in Table 2. For this particular experiment there was a net change of about 12% in X_o over the 673 min observation time and after 800 min the rate of o/p conversion is not much faster than the self-conversion rate. This indicates the H-atom concentration has likely decayed to near zero values over the experimental timescale. A detailed discussion of the parameters extracted from the fits follows in Sec. 4.2.

To explore the temperature dependence of the H-atom catalyzed o/p conversion, we conducted another experiment under similar conditions (initial N_2O concentration and photolysis conditions were consistent), but changed the temperature to 4.00(2) K. Shown in Fig. 3 are the kinetic traces for the o/p conversion experiment conducted on a sample with an initial N_2O concentration of 51(1) ppm that underwent 1.5 min of 216 mW·cm^{-2} photolysis. The sample is initially deposited at ~2.5 K and then the temperature is raised to 4 K prior to photolysis. As shown in Fig. 3, the measured path length is almost constant but increases slightly right after photolysis from an initial value of $d = 0.2071(4)$ cm to around 0.2103(3) cm. These small

Table 2. List of experimental conditions and fitted parameters determined from least-squares fits of Eq. (4) to the X_o data

	Expt. 1	Expt. 2	Expt. 3	Expt. 4	Expt. 5	Expt. 6	Expt. 7	Expt. 8
T, K	1.775(2)	1.792(3)	4.00(2)	4.02(3)	4.04(3)	4.04(2)	4.04(3)	4.02(3)
d, cm	0.209(2)	0.227(2)	0.210(1)	0.223(2)	0.204(1)	0.239(2)	0.248(1)	0.244(1)
photo, min	1.5	3.0	1.5	6.0	6.0	6.0	6.0	6.0
$[N_2O]_0$, ppm	48.4	59.4	50.7	60.8	118.6	38.6	60.7	75.7
$\Delta[N_2O]$, ppm	11.6	26.8	13.5	42.4	79.8	23.9	37.3	44.5
$T_{o/p}$, K	30	30	30	30	30	25	25	20
$k_r n_H(0)$, 10^{-3} min^{-1}	5.9(4)	11.6(3)	5.4(2)	32(2)	25.9(7)	24(5)	20(2)	40(20)
β, 10^{-2}	6.1(2)	7.64(6)	11.0(1)	7.16(6)	11.54(6)	3.0(1)	6.0(1)	4.9(4)
$X_o(0)$, 10^{-2}	2.913(4)	2.861(2)	2.886(3)	2.882(5)	2.814(4)	0.967(3)	0.949(2)	0.178(2)
$[H]_0$, ppm	12.3(8)	24.1(6)	11.2(4)	67(4)	54(1)	50(10)	42(4)	83(42)
R^2	0.994878	0.999031	0.998931	0.997438	0.999314	0.962981	0.991985	0.821781
X_{hcp} *final*	0.58(5)	0.60(2)	1.015(4)	1.012(4)	0.907(4)	1.034(4)	1.016(4)	0.985(3)

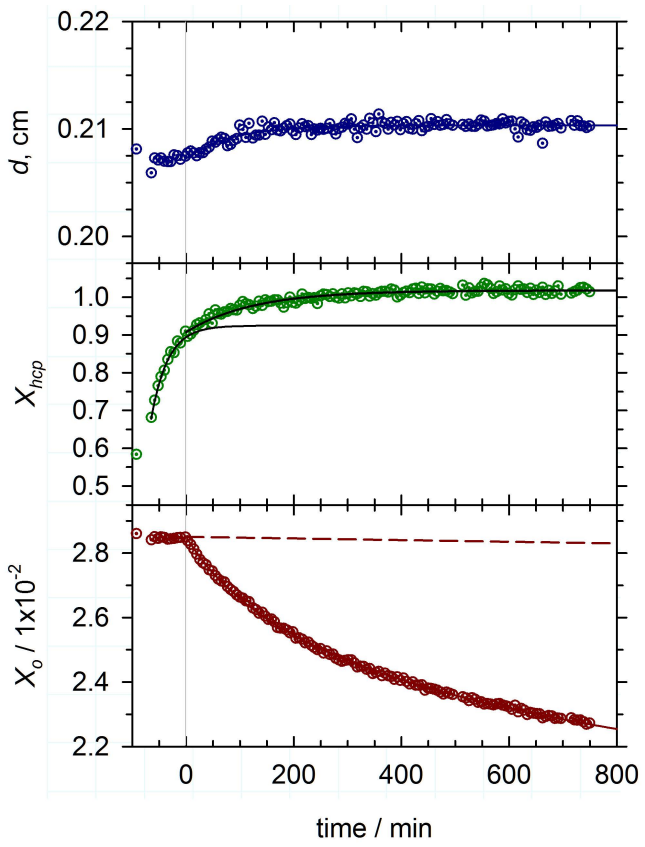

Fig. 3. (Color online) Kinetic traces illustrating the changes in d, X_{hcp}, and X_o for an experiment (Expt. 3) conducted on an annealed sample at 4.00(2) K. The circles are the data points and the lines are fits to the data (see text for details). The sample is photolyzed at 216 mW·cm^{-2} for 1.5 min to initiate the o/p conversion. The dashed line in the plot of X_o shows the predicted X_o time dependence based on the self-conversion rate constant and the initial $X_o(0)$ value. The X_{hcp} data are fit to Eq. (9) with the parameters reported in Table 3.

changes in d likely reflect changes in the absorption coefficient for the $Q_1(0) + S_0(0)$ transition related to crystal structure. As described earlier, double transitions are to first-order insensitive to crystal structure, which is why they are used to measure thickness [33]. However, at higher levels of scrutiny small changes are indeed observed [1,33]. Immediately after deposition (first data point) this crystal had an X_{hcp} value of ~0.591 consistent with the previous sample shown in Fig. 2. Then after raising the temperature to 4 K, the X_{hcp} value exponentially increases to 0.906(7) at near time zero. The X_{hcp} data before photolysis is fit to a simple exponential equation:

$$y = y_0 + A[1 - \exp(-kt)], \tag{9}$$

where y_0 is the quantity being fit at $t = 0$, A is the induced change, and k is the first-order rate constant governing the process. The results of the fit of the X_{hcp} data to Eq. (9) before photolysis are shown as a black line in Fig. 3. We also fit the X_{hcp} data after photolysis to Eq. (9). After photolysis the X_{hcp} value continued to increase to a maximum value of 1.015(4) with a slower first-order rate constant. The fitted parameters for fits of Eq. (9) to the X_{hcp} data after photolysis are collected in Table 3. The fact that the hcp fraction slightly exceeds unity is most likely due to the measurement of d that uses the integral absorption coefficient reported for an X_p = 0.9997 sample. With this, the 1.015(4) value is representative of a fully annealed sample at 4.0 K. Warming the sample to 4 K for the first time after deposition invokes irreversible conversion of fcc to hcp crystal morphologies, as previously observed [33,49]. The final X_{hcp} value also provides an internal check that the integral absorption coefficient used for the $U_1(0)$ transition is consistent with the measured path length and molar volume used in this study (~1.5% error). We will return to the interpretation of the different rates of X_{hcp} conversion before and after photolysis in Sec. 4.4.

What is immediately apparent upon comparison of Figs. 2 and 3 is that the experiment at 4.0 K was more effective at o/p conversion. As shown in Fig. 3, there is a 20% decrease in X_o over a time window of approximately 750 min. Comparison of the fitted parameters in Table 2 helps to explain this difference. The β-parameter for the experiment at 4.0 K is about twice as large as reported for the 1.8 K experiment. We interpret this as an indication that the relative rate constants between catalysis (k_{cc}) and H-atom recombination (k_r) is greater at 4.0 K compared to 1.8 K. The fitted $k_r n_H(0)$ values are nearly equivalent suggesting that the initial H-atom concentrations in both experiments are comparable, and that the k_r value is insensitive to temperature over this range. It is expected that comparable concentrations of H-atoms are produced because similar N_2O concentrations and photolysis conditions are employed in both experiments. One obvious difference is that for the experiment at 4.0 K, the solid has a nearly pure hcp crystal structure (X_{hcp} = 1.015(4)), whereas the experiment at 1.8 K was conducted on an as-deposited

Table 3. Fitted parameters determined from least-squares fits of Eq. (9) to the X_{hcp} data after photolysis

	Expt. 3	Expt. 4	Expt. 5	Expt. 6	Expt. 7	Expt. 8
y_0	0.918(3)	0.933(3)	0.745(3)	1.000(3)	0.891(3)	0.840(2)
A	0.097(3)	0.079(3)	0.162(3)	0.034(3)	0.125(3)	0.145(2)
k, 10^{-3} min^{-1}	7.7(5)	12(1)	4.3(3)	8(2)	11.2(5)	7.0(3)
R^2	0.899416	0.855645	0.959428	0.50916	0.962517	0.96699
σ	0.0077	0.012	0.014	0.015	0.0066	0.0093

crystal with a mixed fcc/hcp crystal morphology. Greater homogeneity in the sample at 4.0 K may increase k_{cc} by allowing the H-atoms to diffuse through greater portions of the sample, or with an accelerated rate.

Experiments conducted at low temperatures ($T \leq 2.4$ K) afford the opportunity to perform simultaneous kinetic measurements on H-atom catalyzed o/p conversion and the H + N_2O tunneling reaction. Shown in Fig. 4 is a comparison of the growth of *trans*-$H^{15}N^{15}N^{18}O$ (here after HNNO) in the two experiments displayed in Figs. 2 and 3. If an H-atom reacts with an N_2O molecule, it ultimately leads to the formation of *trans*-HNNO by the following two-step mechanism:

$$H + N_2O \rightarrow \textit{cis}\text{-HNNO}, \quad (10)$$

$$\textit{cis}\text{-HNNO} \rightarrow \textit{trans}\text{-HNNO}. \quad (11)$$

In the experiment performed at 4.00(2) K, minimal production of *trans*-HNNO is observed (<0.05 ppm), while in the experiment performed at 1.775(2) K, at least ~1.2 ppm of *trans*-HNNO is produced. We have previously reported this strange temperature dependence to the H + N_2O reaction, which only readily occurs below 2.4 K, in highly enriched pH_2 samples [20]. It appears that the same temperature dependence to the H + N_2O reaction is operative in samples with elevated oH_2 concentrations. With the FTIR setup employed in these studies, we cannot monitor the kinetics of the *cis*-HNNO species because the only absorption for this species above 1800 cm^{-1} (NH stretch, 3270.4 cm^{-1}, 2.9 km mol^{-1}) is too weak to detect under

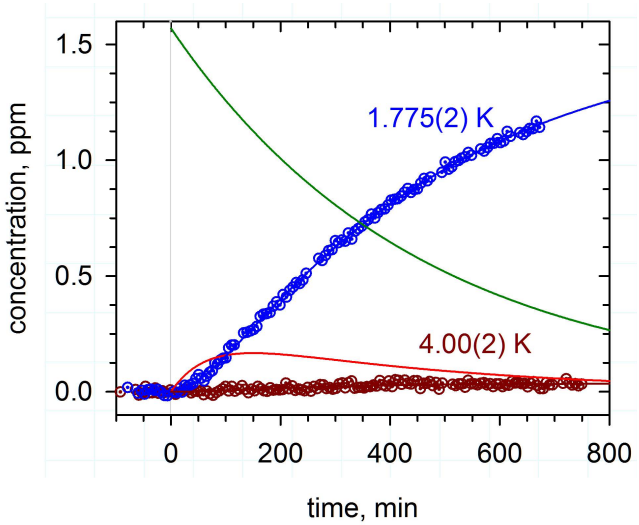

Fig. 4. (Color online) Kinetics traces showing the growth of *trans*-HNNO (A_3) for the two different experiments depicted in Figs. 2 and 3. The blue circles are for the experiment at 1.775(2) K and the brown circles are for the experiment at 4.00(2) K. This shows that H-atoms can decay via reactions with N_2O at 1.8 K, but not at 4.0 K. The green and red lines are the predicted kinetics for A_1 and A_2, respectively, based on least-squares fits of the *trans*-HNNO data to Eq. (14) for the data at 1.775(2) K. See text for details.

these conditions. As discussed previously [20], we can fit the *trans*-HNNO data to analytical expressions developed for first-order consecutive reactions involving one intermediate and two-steps:

$$A_1 \rightarrow A_2, \quad (12)$$

$$A_2 \rightarrow A_3. \quad (13)$$

The assumption here is that we can model the measured reaction kinetics (Eqs. (10) and (11)) with this simple kinetic model. Support for the proposed reaction mechanism is found upon fitting the *trans*-HNNO data to the following kinetic equation:

$$[A_3] = [A_1]_0 \left[1 - e^{-k_{12}t} - \frac{k_{12}}{(k_{13} - k_{12})} (e^{-k_{12}t} - e^{-k_{13}t}) \right], \quad (14)$$

where A_2 and A_3 are associated with *cis*-HNNO and *trans*-HNNO, respectively, and the kinetics involve two first-order rate constants k_{12} and k_{13}. Note that we originally [20] associated A_1 with H-atoms based on the expected pseudo first-order rate expression for Eq. (10), where $k'_{10} = k_{10}$ [N_2O]. Thus, in this analysis we associate k_{12} with the pseudo first-order rate constant (k'_{10}). The results from the fit of Eq. (14) to the *trans*-HNNO data are shown as a blue line in Fig. 4. As can be seen in Fig. 4, Eq. (14) does a very good job at fitting the data. Based on these fitted parameters, the predicted time dependence of *cis*-HNNO and H-atoms are also included in Fig. 4 as red and green lines, respectively, for the reaction at 1.775(2) K. Note the predicted first-order decay in the H-atom concentration deduced from the *trans*-HNNO reaction kinetics conflicts directly with the second-order H-atom decay process predicted by the measured H-atom catalyzed o/p kinetics. This suggests that A_1 is not the H-atom in the proposed mechanism but rather some other species that forms immediately after photolysis and decays with a first-order rate constant as shown by the green line in Fig. 4. We will return to this important finding in Sec. 4.5.

4.2. Ortho-to-para conversion depends on various experimental conditions

We wanted to explore the H-atom catalyzed o/p conversion kinetics under a variety of experimental conditions. Figure 5 contains a plot of the X_o traces from five different experiments that all started with initial X_o values around 0.0295. First, let us test whether the H-atom concentration can be extracted from the fits to these X_o kinetic traces. To examine if the initial H-atom concentration (after photolysis) can be extracted from the fitted $k_r n_H(0)$ parameter let us compare curves (a) and (c) in Fig. 5. These are the two low-temperature kinetic experiments that differ by the length of the photolysis irradiation but have comparable laser powers and initial N_2O concentrations. Just from looking at Fig. 5, it is apparent that these two data sets have basically the same shape but experiment (c) is about

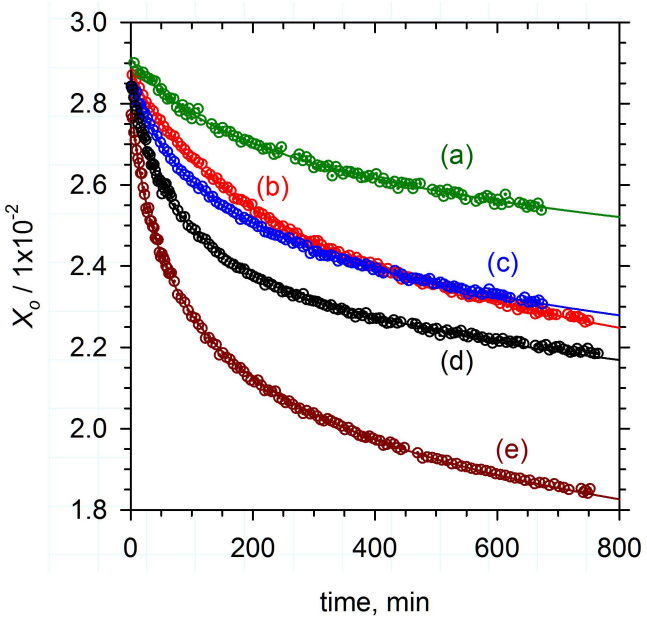

Fig. 5. (Color online) Kinetic traces of X_o for all the different experiments with $X_o(0) = 0.0295$. The data are represented by circles and least squares fits to Eq. (4) are indicated by lines. Note the varying shapes of the curves represent different $k_r n_H(0)$ and β parameters. The labels designate the different experiments: (a) Expt. 1, (b) Expt. 3, (c) Expt. 2, (d) Expt. 4, and (e) Expt. 5. See text for details.

twice as deep as (a). From examination of Table 2 these observations are confirmed. The most significant difference between these two data sets is that the $k_r n_H(0)$ parameter has increased by a factor of 1.97(20) for the experiment involving a 3.0 min laser exposure versus 1.5 min exposure. The β-parameter only varied by ~25% and thus does not change appreciably between the two experiments.

We can now examine the observed trends more quantitatively by measuring correlations between the amount of N_2O photolyzed and the $k_r n_H(0)$ values determined from fits to Eq. (4). Basically, the idea is that the amount of N_2O photolyzed, $\Delta[N_2O] = [N_2O]_{before} - [N_2O]_{after}$, should be highly correlated with the number of H-atoms produced initially. We can measure $\Delta[N_2O]$ using the $2\nu_2$ and $\nu_1+\nu_3$ combination bands of N_2O (see Table 2) and Eq. (8). The initial H-atom concentration after photolysis, $n_H(0)$, is determined from the fitted $k_r n_H(0)$ parameter divided by the literature [12] value for k_r. A correlation plot of all the data measured in this study is presented in Fig. 6 where we compare $\Delta[N_2O]$ with the measured $n_H(0)$ value determined from the least-squares fits to the o/p conversion data. One can see that at small photolysis exposures (low H-atom concentrations) the correlation between the two values is nearly 1:1, as discussed above. For greater photolysis times the correlation shifts to greater amounts of H-atoms being produced. This can be accounted for when one considers the stoichiometry of the O-atoms and H-atoms produced. For instance, following Eq. (1) after the O-atom is ejected it can react with the pH_2 host via the following two-step abstraction mechanism:

$$O + H_2 \rightarrow OH + H, \quad (15)$$

$$OH + H_2 \rightarrow H_2O + H, \quad (16)$$

and thus, every O-atom can produce up to two H-atoms. Alternatively, the O-atom can directly insert into the H_2 molecule and produce no H-atoms. We measure production of both ortho-H_2O and para-H_2O during photolysis which indicates that the ejected O-atom reacts with the pH_2 host. We lack the required time resolution to measure the details of the photoconversion mechanism and have not detected the OH intermediate. Included in Fig. 6 are two limiting cases for 1:1 and 1:2 stoichiometries between the O-atoms and H-atoms plotted as solid lines. All the data falls within these two limiting cases except for the one data point at the $\Delta[N_2O] = 80$ ppm value. This was the most extensive photolysis experiment conducted that started with a N_2O concentration of 119(1) ppm and used a 267(2) mW·cm^{-2} laser flux and 6 min photolysis. The level of correlation displayed in Fig. 6 demonstrates that the parameter $k_r n_H(0)$ can be used as a measure of $n_H(0)$. The rate constant for recombination has been measured previously [12] using ESR spectroscopy and has been shown to vary considerably with X_o. However, in the range between $X_o = 0.01$ to 0.1 the value of k_r changes from $1.9\cdot10^{-20}$ to $3.2\cdot10^{-20}$ cm^3·min^{-1}·mol^{-1} and thus is relatively constant

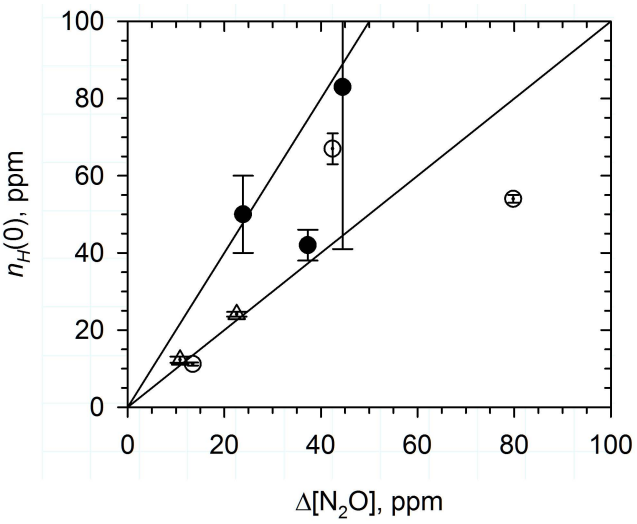

Fig. 6. Correlation plot of Δ $[N_2O]$ versus $n_H(0)$ determined from the fit to the H-atom catalyzed o/p conversion kinetics (both in ppm). Circles are used for high temperature (4.0 K) experiments and triangles for low temperature data (1.8 K). The open circles represent data taken for samples with $X_o(0) = 0.0295$ values and the closed circles are the three experiments conducted at lower $X_o(0)$ values. The error bars represent the errors in the $k_r n_H(0)$ parameter from the least-squares fits. The two lines represent the 1:1 and 1:2 stoichiometries (see text for details) between O-atoms and H-atoms.

over this range (errors implied by number of significant digits). The correlation plot in Fig. 6 therefore provides indirect confirmation that this k_r value is appropriate for our experimental conditions because realistic H-atom concentrations are obtained. This is an important finding because it suggests that by measuring the H-atom catalyzed o/p conversion kinetics we have an indirect measure of the initial H-atom concentration. As we will discuss in Sec. 4.5, extracting the initial H-atom concentration from H-atom reaction studies is problematic and can lead to erroneous values.

4.3. Measuring o/p conversion for different X_o values

We were also interested in examining the o/p conversion kinetics at different initial X_o values. The H-atom recombination rate constant k_r has been measured to decrease by a factor of 3.4 when going from pH_2 solids having X_o = = 0.01 to 0.001, resulting in $k_r = 5.5{\cdot}10^{-21}$ $cm^3{\cdot}min^{-1}{\cdot}mol^{-1}$. Thus, we were interested in whether we could measure a significant change in the β-parameter at lower $X_o(0)$ values. The kinetic traces of X_o are shown in Fig. 7 for three representative crystals with different $X_o(0)$ values. The top trace in Fig. 7 is for a pH_2 solid with $X_o(0)$ = 0.02847(3), the middle trace has $X_o(0)$ = 0.00939(2), and the bottom trace has $X_o(0)$ = 0.00166(2). Note that the general shape of the X_o curves is basically the same except for possibly the bottom trace. This shows that the β-parameter is not changing appreciably between the top and middle traces. Indeed, the biggest difference is just that the magnitude of H-atom catalyzed o/p conversion scales with $X_o(0)$ as expected (see Eq. (2)). The S/N is degraded at the low $X_o(0)$ values because the integrated absorbance of the $Q_1(0) + S_0(1)$ double transition scales with X_o and is weakest at the low X_o values (see Eq. (7)). However, close examination of the bottom trace shows that the X_o value appears to increase right after photolysis. This may be a real effect in that during photolysis some of the H-atoms may recombine to form oH_2. At the higher X_o values this photo-induced change is negligible, but as the oH_2 content decreases it may be possible to initially measure an increase in X_o.

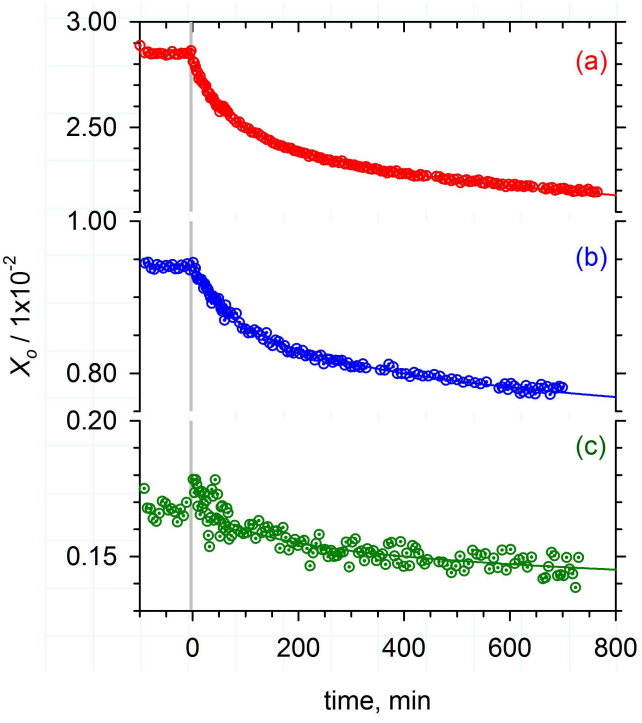

Fig. 7. (Color online) Kinetic traces of X_o for three experiments with different $X_o(0)$ values. The data are represented by circles and least squares fits to Eq. (4) are indicated by lines. The three experiments are: (a) $T_{o/p}$ = 30 K (Expt. 4), (b) $T_{o/p}$ = 25 K (Expt. 7), and (c) $T_{o/p}$ = = 20 K (Expt. 8). Note the general shape of the curves remains similar.

The fact that we do not observe a significant increase in the β-parameter for the pH_2 solid with lowest $X_o(0)$ value may indicate that in addition to changes in k_r with $X_o(0)$, the k_{cc} rate constant also changes with oH_2 concentration. In all the measured H-atom catalyzed o/p kinetics the β-parameter is always significantly less than 0.5 where the two rate constants are equal ($k_{cc} = k_r$); note that the factor of two is considered explicitly by the functional form of Eq. (4). Thus, the rate constant for H-atom catalyzed conversion is significantly smaller than the rate constant for H-atom recombination under these conditions. Both processes are directly linked to the H-atom diffusion constant and thus these differences are meaningful. This too has been observed before and interpreted as evidence that the H-atom does not diffuse isotropically throughout the crystal [10]. It has been speculated that the H-atom diffuses preferably by exchanges with pH_2 molecules and therefore avoids oH_2 molecules present in the solid [10,11]. The significant decrease in k_r for highly enriched pH_2 solids has been interpreted as evidence that H-atoms do not recombine at low oH_2 concentrations, not because the diffusion coefficient is getting smaller, but because the H atoms avoid each other [12]. Thus, at very low X_o values both k_r and k_{cc} may decrease making it difficult to detect a change in the β-parameter. It would be interesting to perform additional experiments at low X_o values to see if the o/p conversion kinetics ever changes substantially.

4.4. Evidence for post-photolysis induced fcc to hcp conversion

Another observation made during these studies was related to changes in X_{hcp} both before and after photolysis. As shown in Fig. 2, as-deposited pH_2 samples do not show systematic changes in X_{hcp} over the whole duration of the experiment while the sample is kept at 1.775(4) K. Indeed this has been observed before qualitatively and discussed in terms of the rapid vapor deposition process [33,49]. In contrast, if the sample is annealed at T = 4.0 K prior to photolysis we observe a first-order kinetic process whereby X_{hcp} increases exponentially to some maximum value. This is shown in Fig. 3, but a clear distinction between the an-

nealing process before and after photolysis is hard to see in this experiment. The experiment depicted in Fig. 3 utilized only a 1.5 min photolysis exposure and based on the o/p conversion fits to Eq. (4), we estimate that only 11.2(4) ppm of H-atoms are produced. However, when we fit the X_{hcp} data to Eq. (9), we measured two different rate constants for the rise in X_{hcp} both before and after photolysis (see Fig. 3). This difference could have been made clearer if more repeated spectra were collected prior to photolysis.

As the study progressed we changed the procedure to better characterize the sample prior to photolysis by taking more repeated scans. Shown in Fig. 8 are two different solids that were both annealed at 4.0 K prior to photolysis. The sample in plot (a) was grown with a $X_o(0)$ value of 0.00166(2) and a N_2O concentration of 76(2) ppm. Now, the different annealing kinetics is clearly distinguished. Prior to photolysis we took 15 repeated scans while the sample was annealed at 4.0 K. We fit that data to Eq. (9) to determine a rate constant for the process. The first data point recorded for the as-deposited sample at low temperature is not included in the fit, but rather only data recorded after the sample temperature is raised to 4.0 K. Note that,

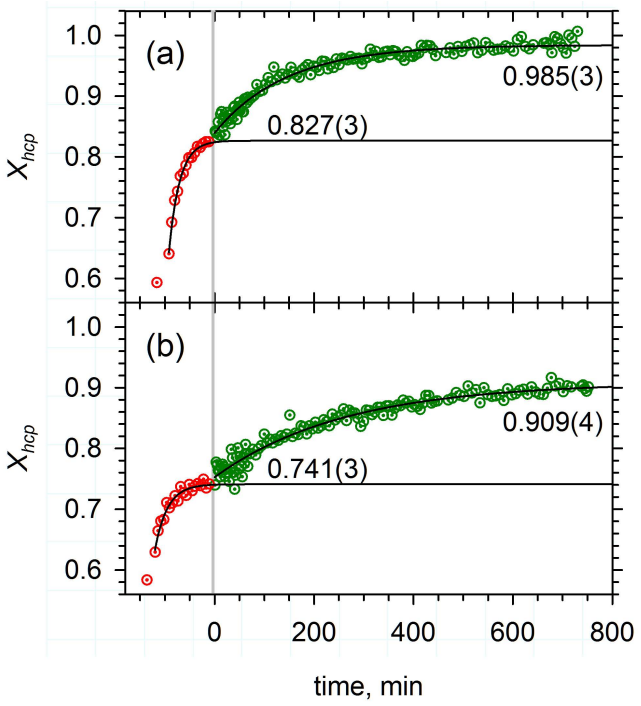

Fig. 8. (Color online) Kinetic data of X_{hcp} for two different experiments with separate least-squares fit to the data before and after photolysis. The circles represent the data and the lines are the results of least squares fits of the data to Eq. (9). All data were recorded at 4.0 K except for the first data point. Expt. 8 is shown in (a) with $X_o(0)$ = 0.00178(2) and $[N_2O]_0$ = 76(1) ppm and Expt. 5 is shown in (b) with $X_o(0)$ = 0.02814(4) and $[N_2O]_0$ = = 119(1) ppm. Note that both samples display additional increases in X_{hcp} after photolysis.

in this case, X_{hcp} reaches a maximum value of 0.827(3) prior to photolysis with a rate constant of $4.6(3)\cdot10^{-2}$ min^{-1} or time constant of 22(1) min. Then after photolysis, the X_{hcp} value starts to grow again with a slower rate constant ($k = 7.0(3)\cdot10^{-3}$ min^{-1}) to a maximum of 0.985(3). It is rationalized that the X_{hcp} value only reaches 0.827(3) prior to photolysis because of the presence of impurities (oH_2 and N_2O) that serve to impede the fcc to hcp conversion process. However, after photolysis continued annealing at 4.0 K is shown to increase the X_{hcp} value from 0.827(3) to 0.985(3). This annealing process triggered by photolysis occurs with a slower rate constant but achieves a higher X_{hcp} value than prior to photolysis. That is, changes produced during photolysis allow the fcc to hcp annealing process to proceed to a greater extent than prior to photolysis. The nature of the induced changes are unclear but could involve conversion of N_2O into N_2 and H_2O and/or the production of H atoms and vacancies that permit further fcc to hcp conversion. We point out that while we do observe a small increase in the sample temperature during photolysis (approximately +0.052 K for (b) in Fig. 8), the change in X_{hcp} continues to happen long after the laser is stopped and thus the changes observed are not likely caused by laser heating during irradiation.

The specific changes in X_{hcp} are different for each experiment, but the same general trend is observed. For example, the sample in plot (b) of Figure 8 was grown with an initial $X_o(0)$ value of 0.02859(2) and N_2O concentration of 119(2) ppm. In this case, X_{hcp} reaches a limiting value of 0.741(3) prior to photolysis and increases to 0.909(4) after photolysis. This sample has both a greater X_o value and N_2O concentration than the sample in plot (a) and, thus, never fully anneals even after photolysis. However, both samples anneal further only after photolysis. This shows that the photolysis process somehow enables further fcc to hcp conversion than was possible pre-photolysis. This could result from photodissociation of N_2O into N_2 and H_2O products which allow for greater conversion. However, the fact that it occurs with a slower rate constant after photolysis could also indicate that H-atoms are playing some role. Perhaps the H-atom catalyzed o/p conversion also facilitates greater fcc to hcp conversion, as the relaxation of an H_2 molecule from ortho to para spin states involves the emission of a roton with energy 170.5 K [3], which ought to be more than sufficient to induce local structural changes.

4.5 Comparison to earlier work

We previously studied H-atom catalyzed o/p conversion at comparable $X_o(0) \approx 0.03$ values using the IR-induced $Cl + H_2 \rightarrow HCl + H$ reaction (see Fig. 9 in Ref. 35). In these previous studies, the H-atoms are generated at much slower rates (0.0154 min^{-1}) by the IR-induced reaction in comparison to the present study using UV photolysis of N_2O (0.17 min^{-1}). Accordingly, in the previous studies we

simply fit the X_o decay kinetics using a single-exponential function (first-order decay). In the course of the present study, we tried to refit the IR-induced Cl + H_2 data using Eq. (4) and found that the residuals from the fits contained systematic deviations indicating that Eq. (4) was not appropriate under these previous experimental conditions. This provides further evidence that one of the requirements of applying Eq. (4) to interpret the H-atom catalyzed o/p conversion data is that the H-atoms are generated quickly to give a precise start time to the measured kinetics. Conversely, if the data in the present study are fit to a single-exponential decay function, the residuals also show large systematic deviations. This again supports the idea that Eq. (4), developed by Shevtsov and co-workers [10], is consistent with the measured H-atom catalyzed o/p kinetics and that the fitted parameters correspond to physical properties of the competing time dependent processes of H-atom catalyzed o/p conversion and H-atom decay.

The correlation plot shown in Fig. 6 is constructed using the previous measurements of k_r. The k_r rate constant for H-atom recombination has been measured in several studies [6–14] under varying conditions and shows a non-monotonic dependence on X_o. We constructed Figure 6 using the k_r value measured at X_o = 0.01 and reported by Kumada *et al.* [12]. This shows that the initial H-atom concentrations, $n_H(0)$, calculated by dividing the fitted $k_r n_H(0)$ parameters by the literature value of k_r are consistent with the magnitude of the N_2O concentration decrease produced upon photolysis. This correlation between the H-atom catalyzed o/p kinetics and IR spectroscopy therefore supports the assertion that Eq. (4) reproduces the data satisfactorily and the fitted parameters correspond to physical properties, such as $n_H(0)$. Since both T = 1.8 and 4.0 K data are included in Fig. 6, this also suggests that k_r is not strongly dependent on temperature over this range for these X_o values, supporting previous claims [10]. Clearly, a direct measurement of $n_H(0)$ based on ESR spectroscopy is a more quantitative determination of the H-atom concentration. However, the correlation data presented here in Fig. 6 supports our claim that we can estimate the $n_H(0)$ values achieved under our conditions. For example, it shows that H-atom concentrations on the order of ~100 ppm are possible using *in situ* N_2O photolysis.

Furthermore, the fact that the H-atom catalyzed o/p conversion data are well reproduced by Eq. (4) supports the idea that the H-atom decay is dominated by H-atom recombination. In the derivation of Eq. (4) it is assumed that the H-atoms decay by second-order H-atom recombination (e.g., Eq. (3)). Thus, we can plot the H-atom decay as a function of time that is consistent with the measured o/p conversion kinetics for any specific experiment. Shown in Fig. 9 is the predicted H-atom time dependence for the first experiment conducted at 1.775(2) K on an as-deposited sample with an initial N_2O concentration of 48(1) ppm. Under these conditions, we estimate the production of 12.3(8) ppm of H-atoms from the fitted $k_r n_H(0)$ parameter. However, as also shown in Fig. 4, based on the kinetic fits to the production of *trans*-HNNO, only 1.57(3) ppm of H-atoms react with N_2O under these conditions. Based on fitting the *trans*-HNNO growth kinetics, we show in Fig. 9 the decay of the H-atoms that is consistent with the measured H-atom reaction kinetics; first-order decay from an initial value of 1.57(3) ppm. The significant discrepancy between the two predicted H-atom decay curves (magnitude and shape) illustrated in Fig. 9 underscores the conflict between the interpretation of the H-atom catalyzed o/p kinetics and the kinetics of the H + N_2O reaction. If the H-atom decay is dominated by H-atom recombination, then the second-order decay in the H-atom concentration with time should be reflected in the H + N_2O reaction kinetics, and it is not. If instead the H-atom decay is dominated by the H + N_2O reaction, then why do so few H-atoms react with N_2O to form *trans*-HNNO? One possibility is that the rate determining step for the H + N_2O reaction does not involve diffusion of the reagents (H + N_2O), while diffusion is the rate determining step in the H-atom recombination reaction. Even more intriguing, these two conflicting kinetic measurements are performed on the same sample ruling out the possibility of different experimental conditions.

This same discrepancy was originally identified in the study of the H + NO → HNO reaction by Fushitani and Momose [19]. If they assumed that the H + NO reaction was diffusion limited then the $k_{H–NO}$ rate constant that they measured should equate with the k_r rate constant determined

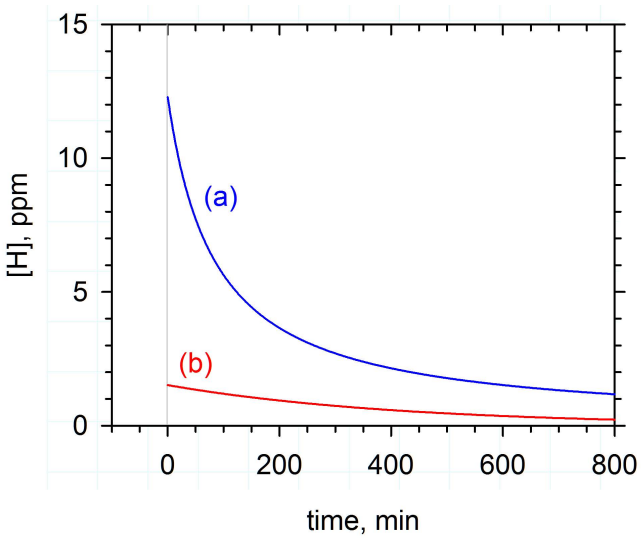

Fig. 9. Plots of the predicted H-atom decay kinetics for the experiment depicted in Fig. 2 based on the fits to (a) H-atom catalyzed o/p conversion kinetics and (b) *trans*-HNNO growth kinetics. Based on this study we believe the H-atom decay kinetics determined from the (a) H-atom catalyzed o/p conversion kinetics is the correct depiction of the time dependent H-atom concentration and that trace (b) represents the decay of some other chemical species. See text for details.

from H-atom recombination studies, properly taking into account the stoichiometric coefficient of two in the recombination reaction. However, they measure a $k_{H–NO}$ value of $6.22\cdot10^{-19}$ $cm^3\cdot min^{-1}$ which is two-orders of magnitude larger than the $5.5\cdot10^{-21}$ $cm^3\cdot min^{-1}$ value of k_r at X_o = = 0.001 determined from ESR studies. They reasoned that part of the discrepancy may be due to differences in crystal quality (X_o, defects) in the two distinct experimental studies. They also pointed out that the intermolecular interaction energy between an H-atom and NO is approximately 200 times stronger than between two H-atoms and that this could affect the H-atom diffusion rate. Subsequent work from our laboratory has shown that the assumption that the H + NO rate constant reflects in some way the H-atom diffusion rate is not supported by experiment [23]. The rate constant measured for the H + NO reaction does not depend on the NO concentration as it must to be able to extract the diffusion limited rate constant from the pseudo first-order growth of HNO in the conventional manner.

The measurements of H-atom catalyzed o/p conversion kinetics presented in this study show that even in chemically doped pH_2 solids the dominant decay mechanism of the H-atoms is recombination. Fits of the o/p conversion data to Eq. (4) give reasonable $n_H(0)$ values and this equation is very capable of modeling the measured o/p conversion kinetics under various starting conditions. These measurements clearly indicate that the proposed mechanism for the H + N_2O reaction is incomplete and not consistent with the H-atom catalyzed o/p conversion kinetics. The rate determining step is not diffusion of the H-atom to an adjacent lattice site of the N_2O reactant as indicated by Eq. (7), but rather the measured reaction kinetics do not reflect the H-atom diffusion rate. This surprising result that a solid-state reaction is not diffusion limited has previously been hinted at in the case of the H + NO reaction, but it is only clear now that we have an independent (albeit indirect) measurement of the H-atom concentration. The magnitude and shape of the H-atom decay curve does not match the assumed H-atom decay curve from the H + N_2O reaction kinetics. The ramifications of this finding are two-fold: (1) a new mechanism for the H + N_2O reaction needs to be developed that is consistent with the measured H-atom concentration profiles measured indirectly from the o/p conversion kinetic data and (2) H-atom diffusion is likely more facile than previously thought based on the H-atom recombination studies. Specifically for this study, the H + N_2O reaction is not diffusion limited in the normal sense and the H-atom is not species A_1 in the proposed two-step mechanism. However, it remains to be seen if this is only true for the H + N_2O reaction, or applicable in a broader sense. Further, for reaction studies in highly enriched pH_2 samples, the basic reaction mechanisms may change again because it is known that the H-atom recombination rate constant depends strongly on X_o.

5. Summary

We have measured the H-atom catalyzed o/p conversion of eight different N_2O doped pH_2 samples that demonstrate fits to the o/p conversion kinetics can be used to extract information about the rate of H-atom recombination and the rate of catalyzed o/p conversion. Specifically, we show that all data sets can be fit to an analytical expression involving only three physical parameters. Most importantly, we have shown that one of these parameters, namely the $k_r n_H(0)$ parameter, can be used to estimate the concentration of H-atoms produced right after photolysis. Moreover, that the high quality of the fits to the data suggests that the majority of H-atoms decay through the second-order process of H-atom recombination. Our results are also consistent with the earlier ESR measurements in that we do not observe a strong temperature dependence to the H-atom recombination rate constant over this range [10,11] and the amount of H-atom catalyzed o/p conversion is significantly less than expected if the H-atoms are to randomly diffuse throughout the solid hydrogen lattice [11].

The observation that the H-atom catalyzed o/p conversion is consistent with second-order decay in the H-atom concentration helps constrain the interpretation of the reaction kinetics of the H + N_2O reaction that we previously reported [20]. Basically, the discrepancy in the H-atom decay curve that these studies predict based on either the o/p conversion or reaction kinetics allows us to see that we have been incorrectly interpreting the H + N_2O reaction kinetics. This has been suggested previously because in some cases the data show that the measured reaction rate constant does not scale linearly with the concentration of the chemical reactant as it must to be diffusion-limited in the normal sense [23,24]. Therefore, we feel the present studies that permitted the o/p conversion and reaction kinetics to be measured simultaneously were a significant breakthrough in the interpretation of the H + N_2O reaction kinetics. The challenge now is to come up with a different mechanism that explains the H + N_2O reaction kinetics. It also would be interesting to reproduce these H-atom catalyzed o/p conversion experiments with other closed-shell precursor molecules such as CH_3OH.

Acknowledgments

This work was sponsored in part by the Chemistry Division of the US National Science Foundation (CHE 13–62497).

1. J. Van Kranendonk, *Solid Hydrogen, The Theory of Properties of Solid H_2, HD, and D_2*, Plenum Press, New York (1983).
2. *Physics of Cryocrystals*, V.G. Manzhelii, Yu.A. Freiman, M.L. Klein, and A.A. Maradudin (eds.), AIP Press, Woodbury, New York (1997).
3. I.F. Silvera, *Rev. Mod. Phys.* **52**, 393 (1980).

4. L.I. Amstutz, J.R. Thompson, and H. Meyer, *Phys. Rev. Lett.* **21**, 1175 (1968).
5. R. Oyarzun and J. Van Kranendonk, *Phys. Rev. Lett.* **26**, 646 (1971).
6. T. Miyazaki, K.-P. Lee, K. Fueki, and A. Takeuchi, *J. Phys. Chem.* **88**, 4959 (1984).
7. T. Miyazaki, S. Mori, T. Nagasaka, J. Kumagai, Y. Aratono, and T. Kumada, *J. Phys. Chem. A* **104**, 9403 (2000).
8. A.V. Ivliev, A.Y. Katunin, I.I. Lukashevich, V.V. Sklyarevskii, V.V. Suraev, V.V. Filippov, N.I. Filippov, and V.A. Shevtsov, *JETP Lett.* **36**, 472 (1982).
9. A.Y. Katunin, I.I. Lukashevich, S.T. Orozmamatov, V.V. Sklyarevskii, V.V. Suraev, V.V. Filippov, N.I. Filippov, and V.A. Shevtsov, *JETP Lett.* **34**, 357 (1981).
10. V. Shevtsov, A. Frolov, I. Lukashevich, E. Ylinen, P. Malmi, and M. Punkkinen, *J. Low Temp. Phys.* **95**, 815 (1994).
11. T. Kumada, S. Mori, T. Nagasaka, J. Kumagai, and T. Miyazaki, *J. Low Temp. Phys.* **122**, 265 (2001).
12. T. Kumada, M. Sakakibara, T. Nagasaka, H. Fukuta, and J. Kumagai, *J. Chem. Phys.* **116**, 1109 (2002).
13. T. Kumada, *Phys. Rev. B* **68**, 052301 (2003).
14. T. Kumada, Y. Shimizu, T. Ushida, and J. Kumagai, *Radiat. Phys. Chem.* **77**, 1318 (2008).
15. C.M. Edwards, N.S. Sullivan, and D. Zhou, *Phys. Scr.* **19**, 458 (1987).
16. E.G. Kisvarsanyi and N.S. Sullivan, *Phys. Rev. B* **51**, 3462 (1995).
17. D. Zhou, C.M. Edwards, and N.S. Sullivan, *Phys. Rev. Lett.* **62**, 1528 (1989).
18. K. Yoshioka, P.L. Raston, and D.T. Anderson, *Int. Rev. Phys. Chem.* **25**, 469 (2006).
19. M. Fushitani, and T. Momose, *Fiz. Nizk. Temp.* **29**, 985 (2003) [*Low Temp. Phys.* **29**, 740 (2003)].
20. F.M. Mutunga, S.E. Follett, and D.T. Anderson, *J. Chem. Phys.* **139**, 151104 (2013).
21. L.O. Paulson, F.M. Mutunga, S.E. Follett, and D.T. Anderson, *J. Phys. Chem. A* **118**, 7640 (2014).
22. W.R. Wonderly, and D.T. Anderson, *J. Phys. Chem. A* **118**, 7653 (2014).
23. M. Ruzi, and D.T. Anderson, *J. Phys. Chem. A* **119**, 12270 (2015).
24. M.E. Balabanoff, M. Ruzi, and D.T. Anderson, *Phys. Chem. Chem. Phys.* **20**, 422 (2018).
25. J.C. Amicangelo and Y.-P. Lee, *J. Chem. Phys.* **149**, 204304 (2018).
26. K.A. Haupa, B.A. Johnson, E.L. Sibert III, and Y.-P. Lee, *J. Chem. Phys.* **147**, 154305 (2017).
27. K.A. Haupa, A.G.G.M. Tielens, and Y.-P. Lee, *Phys. Chem. Chem. Phys.* **19**, 16169 (2017).
28. T. Kumada, N. Kitagawa, T. Noda, J. Kumagai, Y. Aratono, and T. Miyazaki, *Chem. Phys. Lett.* **288**, 755 (1998).
29. A.F. Andreev, *Sov. Phys. Usp.* **19**, 137 (1976).
30. A.F. Andreev, and I.M. Lifshitz, *Sov. Phys. JETP* **29**, 1107 (1969).
31. S. Tam,and M.E. Fajardo, *J. Chem. Phys.* **108**, 4237 (1998).
32. S. Tam and M.E. Fajardo, *Rev. Sci. Instrum.* **70**, 1926 (1999).
33. S. Tam and M.E. Fajardo, *Appl. Spectrosc.* **55**, 1634 (2001).
34. L. Andrews, and X. Wang, *J. Chem. Phys.* **121**, 4724 (2004).
35. P.L. Raston, S.C. Kettwich, and D.T. Anderson, *Fiz. Nizk. Temp.* **36**, 495 (2010) [*Low Temp. Phys.* **36**, 392 (2010)].
36. L. Abouaf-Marguin, and A.-M. Vasserot, *Chem. Phys. Lett.* **460**, 82 (2008).
37. L. Abouaf-Marguin and A.-M. Vasserot, *Fiz. Nizk. Temp.* **37**, 456 (2011) [*Low Temp. Phys.* **37**, 357 (2011)].
38. L. Abouaf-Marguin, A.-M. Vasserot, and A. Lekic, *Chem. Phys. Lett.* **470**, 228 (2009).
39. L. Abouaf-Marguin, A.-M. Vasserot, and C. Pardanaud, *J. Chem. Phys.* **130**, 054503 (2009).
40. L. Abouaf-Marguin, A.-M. Vasserot, C. Pardanaud, J. Stienlet, and X. Michaut, *Chem. Phys. Lett.* **454**, 61 (2008).
41. V. Shevtsov, A. Scherbakov, P. Malmi, E. Ylinen, and M. Punkkinen, *J. Low Temp. Phys.* **104**, 211 (1996).
42. V. Shevtsov, E. Ylinen, P. Malmi, and M. Punkkinen, *Phys. Rev. B* **62**, 12386 (2000).
43. J.A. Schmidt, M.S. Johnson, U. Lorenz, G.C. McBane, and R. Schinke, *J. Chem. Phys.* **135**, 024311 (2011).
44. G.S. Selwyn and H.S. Johnston, *J. Chem. Phys.* **74**, 3791 (1981).
45. R. Schinke, *Chem. Phys.* **399**, 142 (2012).
46. P.L. Raston, S.C. Kettwich, and D.T. Anderson, *J. Mol. Spectrosc.* **310**, 72 (2015).
47. J.I. Steinfeld, J.S. Francisco, and W.L. Hase, *Chemical Kinetics and Dynamics*, Prentice Hall, Upper Saddle River, New Jersey (1999).
48. M.E. Fajardo, in: *Physics and Chemistry at Low Temperatures*, L. Khriachtchev (ed.), Pan Stanford Publishing, Singapore (2011), p. 167.
49. S. Tam, M.E. Fajardo, H. Katsuki, H. Hoshina, T. Wakabayashi, and T. Momose, *J. Chem. Phys.* **111**, 4191 (1999).
50. W. Ivancic, T.K. Balasubramanian, J.R. Gaines, and K.N. Rao, *J. Chem. Phys.* **74**, 1508 (1981).
51. A.P. Mishra, T.K. Balasubramanian, R.H. Tipping, and Q. Ma, *J. Mol. Spectrosc.* **695–696**, 103 (2004).
52. M. Okumura, M.-C. Chan, and T. Oka, *Phys. Rev. Lett.* **62**, 32 (1989).
53. R.A. Steinhoff, K.V.S.R. Apparao, D.W. Ferguson, K.N. Rao, B.P. Winnewisser, and M. Winnewisser, *Can. J. Phys.* **72**, 1122 (1994).
54. J. Van Kranendonk, *Can. J. Phys.* **38**, 240 (1960).
55. H.P. Gush, W.F.J. Hare, E.J. Allin, and H.L. Welsh, *Can. J. Phys.* **38**, 176 (1960).
56. B. Moore, P. Djuricanin, and T. Momose, *J. Phys. Chem. Lett.* **9**, 6475 (2018).
57. N.N. Galtsov, A.I. Prokhvatilov, G.N. Shcherbakov, and M.A. Strzhemechny, *Fiz. Nizk. Temp.* **29**, 1036 (2003) [*Low Temp. Phys.* **29**, 784 (2003)].
58. L.S. Rothman, I.E. Gordon, Y. Babikov, A. Barbe, D.C. Benner, P.F. Bernath, M. Birk, L. Bizzocchi, V. Boudon, L.R. Brown, A. Campargue, K. Chance, E.A. Cohen, L.H. Coudert, V.M. Devi, B.J. Drouin, A. Fayt, J.-M. Flaud, R.R. Gamache, J.J. Harison, J.-M. Hartmann, C. Hill, J.T. Hodges, D. Jacquemart, A. Jolly, J. Lamouroux, R.J. Le Roy, G. Li, D.A. Long,

O.M. Lyulin, C.J. Mackie, S.T. Massie, S. Mikhailenko, H.S.P. Muller, O.V. Naumenko, A.V. Nikitin, J. Orphal, V.Perevalov, A. Perrin, E.R. Polovtseva, C. Richard, M.A.H. Smith, E. Stravikova, K. Sung, S. Tashkun, J. Tennyson, C.C. Toon, V.G. Tyuterev, and G. Wagner, *J. Quant. Spec. Rad. Trans.* **130**, 4 (2013).

59. K.A. Peterson, and J.S. Francisco, *J. Chem. Phys.* **134**, 084308 (2011).

Орто-пара конверсія у твердому молекулярному водні, яка каталізована атомами водню

A.I. Strom, K.L. Fillmore, D.T. Anderson

ІЧ спектроскопія використовується для дослідження процесу орто-пара (о/п) конверсії в зразках твердого молекулярного водню, які доповані малими концентраціями (10–50 ppm) атомів водню (Н-атомів) в якості домішки. Н-атоми генеруються з використанням фотолізу *in situ* 193 нм домішкових молекул N_2O. Для кристалів водню з відносно низькими початковими долями орто-H_2 ($X_o \leq 0{,}03$) кінетика конверсії о/п при температурах 1,8 та 4,0 К відповідає кінетичним рівнянням, отриманим раніше для каталізованої атомами водню о/п конверсії. Виміряна кінетика о/п конверсії, яка каталізована Н-атомами, показує, що Н-атоми в цих умовах рухливі відповідно до попередніх вимірів ЕСР. Припускається, що Н-атоми дифундують за допомогою механізму квантового тунелювання, який описується як хімічна дифузія. Детальна підгонка виміряних кінетичних даних щодо о/п конверсії дозволяє визначити початкову концентрацію Н-атомів після фотолізу, виходячи з літературних значень константи швидкості рекомбінації Н-атомів ($H + H \rightarrow H_2$). Виміряна кінетика о/п перетворення показує, що спостережена о/п конверсія набагато менше, ніж очікувалося виходячи з раніше виміряної константи швидкості рекомбінації Н-атомів. Таким чином, слід припустити, що Н-атоми не дифундують випадковим чином крізь кристал, а переміщуються, скоріше, переважно в області з високим вмістом пара-водню. Оцінені концентрації Н-атомів в цьому дослідженні узгоджуються з попередніми вимірюваннями ЕСР, але суперечать кінетичним дослідженням реакцій Н-атомів з різними домішками, такими як N_2O.

Ключові слова: твердий водень, квантове тверде тіло, орто-пара конверсія, квантова дифузія, конверсія ядерних спинів, квантово-механічне тунелювання.

Орто-пара конверсия в твердом молекулярном водороде, катализированная атомами водорода

A.I. Strom, K.L. Fillmore, D.T. Anderson

ИК спектроскопия используется для исследования процесса орто-пара (о/п) конверсии в образцах твердого молекулярного водорода, допированных малыми концентрациями (10–50 ppm) атомов водорода (Н-атомов) в качестве примеси. Н-атомы генерируются с использованием фотолиза *in situ* 193 нм примесных молекул N_2O. Для кристаллов водорода с относительно низкими начальными долями орто-H_2 ($X_o \leq 0{,}3$) кинетика конверсии о/п при температурах 1,8 и 4,0 К соответствует кинетическим уравнениям, полученным ранее для катализируемой атомами водорода о/п конверсии. Измеренная кинетика о/п конверсии, катализируемая Н-атомами, показывает, что Н-атомы в этих условиях подвижны в соответствии с предыдущими измерениями ЭСР. Предполагается, что Н-атомы диффундируют с помощью механизма квантового туннелирования, который описывается как химическая диффузия. Детальная подгонка измеренных кинетических данных о/п конверсии позволяет извлечь начальную концентрацию Н-атомов после фотолиза, исходя из литературных значений константы скорости рекомбинации Н-атомов ($H + H \rightarrow H_2$). Измеренная кинетика о/п конверсии показывает, что наблюдаемое о/п превращение намного меньше, чем ожидалось исходя из ранее измеренной константы скорости рекомбинации Н-атомов. Таким образом, следует предположить, что Н-атомы не диффундируют случайным образом сквозь кристалл, а перемещаются, скорее, преимущественно в области с высоким содержанием пара-водорода. Оцененные концентрации Н-атомов в настоящем исследовании согласуются с предыдущими измерениями ЭСР, но противоречат кинетическим исследованиям реакций Н-атомов с различными примесями, такими как N_2O.

Ключевые слова: твердый водород, квантовое твердое тело, орто-пара конверсия, квантовая диффузия, конверсия ядерных спинов, квантово-механическое туннелирование.